Ramp-Rate Control for Mitigation of Solar PV Fluctuations with Hybrid Energy Storage System

G. V. Brahmendra Kumar and K. Palanisamy*

School of Electrical Engineering, Vellore Institute of Technology, Vellore, 632014, India
E-mail: brahmendrakumar.g@gmail.com; kpalanisamy@vit.ac.in
**Corresponding Author*

Received 29 November 2021; Accepted 10 January 2022;
Publication 27 February 2023

Abstract

This paper proposes a ramp-rate control (RRC) for mitigation of solar PV fluctuations with a hybrid energy storage system (HESS). The highly fluctuating primary energy source causes photovoltaic (PV) generators to suffer from variable output capacity. Such variations can lead to instability in power systems and problems with power quality due to large PV penetration. The role of energy storage devices (ESSs) as a fluctuation compensator is suggested to minimize these issues using RRC. Distributed Generation Systems (DGs) have become a key challenge as the disruption of DG from the grid during faults results in severe difficulties such as power outages and voltage flickers. Low voltage ride through (LVRT) is a promising method for supplying reactive power under low voltage conditions. The proposed method will enable dynamic control of integrated battery storage (BS) to mitigate power fluctuations during the day while simultaneously charging or discharging the integrated super-capacitor (SC) storage to control sudden variations in a BS to a certain magnitude. A system for exchanging energy between the BS and the SC storage provides uninterrupted control of the rapid

Distributed Generation & Alternative Energy Journal, Vol. 38_3, 817–840.
doi: 10.13052/dgaej2156-3306.3835

fluctuations of the passing cloud. The storage capacity savings are evaluated by using the RRC for the smoothing impact of geographical deflection on PV power production. Simulations conducted with real operational PV power output data taken every 1 s from the power plant during one year confirm the validity of the model. The OP-5700 HIL test-bench is used for the real-time results.

Keywords: PV system, fluctuations, ramp-rate control, battery storage, supercapacitor, fault-ride through.

1 Introduction

More than 25 years ago, concerns about the potential for PV output variability due to seasonal clouds were raised, and the increasing PV penetration levels have now attracted broad interest and attention. With the rise in PV power fluctuations on the grid, power quality and reliability can have a negative impact [1, 2]. The grid typically absorbs power fluctuations of less than 10 minutes as frequency variations. This is a particular issue in relatively small networks, for example, islands with high rates of penetration, because of the intrinsically restricted smoothing outcome from the combination of geographically distributed PV plants [3–5].

While the decreasing cost of electronic power devices and the breakthrough of new energy storage technologies allow for the integration of ESS into renewable energy systems (RESs), their capacity depends heavily on the cost per power unit. Commercial and industrial acceptance is prohibitively expensive. In order to meet the required specifications, it is essential to develop a method to optimize the size and operation of an ESS [6–8]. New grid codes have been provided by the TSOs, including new requirements that promote TSO responses suitable for detrimental variations in irradiance, i.e., variations of less than 10 minutes on a time scale. Such requirements include determining the maximum power variance ramps used by intermittent plants to supply power into the network [9, 10].

In places of high PV penetration and small grids, like islands, this risk is relatively significant. Currently, new grid standards in Puerto Rico are more stringent and limit the maximum variability during a time period, normally 1 min, to a certain value of 10% depending on the power generated by the transformer of the PV plant [11]. Moreover, the target for the regulations is much more stringent in other countries, like Mexico, at approximately 1–5%/min. Unlike conventional power systems, PV power generators are not

dynamic enough to affect the balance between production and consumption at any given time. To set these values, the currently increasing power levels for thermal power stations, which are at between 2.5% and 4% of nominal power/min, are usually used as a benchmark for manageable generation. Intermittent power generation requires a quick response from the rest of the system if it has sufficient control capacity [12, 13]. In this scenario, PV power variations are more significant than these standards, and therefore, a certain type of ESS is necessary to meet these requirements. Increasing the price of electricity generated by PV is considered a key aspect in constructing new PV plants. Consequently, methods to comply with the regulations are absolutely necessary, thus utilizing the minimum storage capacity possible [14, 15].

In general, the majority of hybrid storage studies are presented in the literature on wind energy. There has been a recent movement to use solar energy applications with HESSs [16, 17]. The key drawback of the approach proposed in [16] is that the ESS should always operate to satisfy the demand for output capacity. The reference power output tends to vary from that which results in the continuous operation of the HESS. This may increase the system's operating costs. In 2015, for large-scale solar power supply, a multi-objective optimization algorithm for device failure and power limits of HESS was introduced. However, there is no discussion about voltage regulation to enhance the voltage profile of the power supply system. In [18], the economic cost of installing ESS has been analysed to facilitate the variation in short-term PV production as a function of the maximum allowable ramp rate, intermittence time scale, and PV resource dispersion. Geographic dispersion has been shown to result in significant ESS savings by smoothing out PV fluctuations. However, there are no methodologies available to calculate ESS to smoothen the short-term variability of PV power output.

Currently, ramp-rate control is the most promising technique to mitigate the intermittent PV power fluctuations. There are also other solutions available, but these go beyond variations in short time periods and require a much larger ESS [19, 20]. One of the benefits of the moving average method is lower ESS capacity at the cost of increasing energy through the ESS, which results in increased losses and cycle degradation [21]. Some studies [22, 23] indicate that the forecast and the clearness index can be used to solve this problem. The main benefit of RRC is that it only operates if the fluctuation is greater than the maximum acceptable ramp value, which results in less cycling degradation.

Figure 1 represents the grid-connected PV system HESS. Figure 1 consists of a high and lower energy density device such as a battery and SC. The

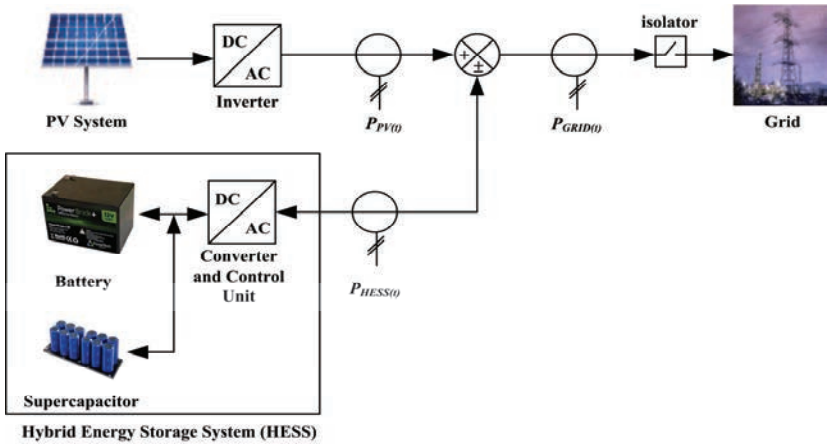

Figure 1 Grid connected PV system with HESS.

li-ion battery and SC storage systems for this research are combined in order to produce a HESS. The battery storage will mitigate slow fluctuations, and the rapid changes are alleviated with SC storage. Based on hybrid topology and 24-hour energy availability (sun irradiation, demand, and cloud ramping events), both slow and fast variations will be calculated for the energy storage capacity (or size).

The paper proposes a method to mitigate the fluctuations in PV output through ESS for 500 kW_p solar PV using RRC. The purpose of ESS is to store surplus energy when the sun is not available and reduce the sudden variation of voltage. The proposed system uses the proper algorithm during ramping and post-ramping events to monitor the PV-RR output production. The ESS is controlled by ramp-down or ramp-up events, relying on the inverse characteristic of the PV-RR required relative to the PV-RR output panel to increase mitigation performance. An efficient power-sharing approach is needed for integrated solar PV systems and HESS. Because of the increased penetration of solar PV panels in the distribution system, the cost of energy storage has decreased significantly, and limitations can be overcome by implementing an effective energy management technology. The PV system is incorporated into the grid and injects reactive power to ensure stable grid voltage in the event of fault conditions. Hence, the PV system delivers real power as quickly as possible once the grid voltage reaches its nominal value so that the entire system can recover from its power imbalance. The following paper is presented as follows: Section 2 discusses the ESS design requirements for RRC, and the control strategy for the proposed system is explained in

Section 3. Section 4 presented the simulation and HIL test-bench results, and Section 5 is the conclusion.

2 ESS Design Requirements for RRC

There are power variations well beyond the limits of standard PV plants, as shown in Table 1. There have been recorded normal and severe variations of up to 70 and 90%/min, shown in Figures 2 and 3. Therefore, in order to smoothen the PV output power, compliance with these regulations includes the combination of PV generators with ESS technologies that can be used to add/subtract power from the PV supply [24, 25]. The maximum speed of a cloud, which varies depending on the direction and location, is enclosed by the PV plant.

The PV plant can be covered with maximum cloud speed and can generate the maximum power in the shortest amount of time under the most extreme conditions. In Equation (1), τ is an empirically correlated time constant with the shortest dimension of the perimeter of the PV plant illustrated in Figure 4,

Table 1 Irradiation profile for the year 2019–20

Days	Sep-19	Oct-19	Nov-19	Dec-19	Jan-20	Feb-20	Mar-20	Apr-20	May-20	Jun-20	Jul-20	Aug-20
(Dialy Avg.) 1	348.331	215.251	487.036	395.029	367.076	461.773	503.894	484.818	420.957	471.438	323.491	442.157
2	452.425	391.899	466.682	312.025	418.457	452.180	499.131	432.063	481.715	470.632	224.942	427.992
3	431.595	491.02	490.846	280.717	439.404	484.251	530.017	448.422	461.454	465.555	383.784	435.056
4	251.456	478.703	505.622	270.296	461.751	474.023	500.899	472.148	414.16	139.854	442.238	371.706
5	454.677	422.343	424.189	426.116	475.962	399.581	416.874	494.961	447.007	397.88	363.19	337.111
6	473.459	425.761	320.062	441.247	483.457	449.935	430.394	537.204	284.734	360.625	357.261	370.326
7	530.453	424.712	492.596	450.643	435.136	455.888	353.313	411.404	365.409	434.495	356.682	339.054
8	551.366	185.539	497.994	453.469	353.225	466.468	495.707	480.237	354.013	396.332	494.429	398.933
9	454.777	176.772	502.929	453.796	411.29	458.792	429.863	385.522	430.856	393.22	308.758	113.674
10	144.601	394.343	489.302	423.17	394.501	465.847	473.915	449.721	57.227	250.442	452.075	399.603
11	180.481	380.756	498.642	391.592	431.192	478.305	547.491	548.708	498.125	296.375	328.328	415.105
12	211.335	450.499	441.362	442.97	436.908	459.281	519.771	557.835	481.666	219.387	419.11	350.397
13	126.756	505.602	0.535	360.874	337.135	469.488	494.56	509.865	481.908	271.807	311.671	141.811
14	195.532	545.908	275.695	99.885	137.047	450.94	469.157	458.905	440.224	288.136	290.142	257.805
15	173.065	540.426	343.035	398.873	399.829	478.1	404.94	497.506	401.39	264.052	245.643	375.116
16	276.922	450.502	389.848	370.792	435.212	491.857	440.359	493.438	483.279	385.836	169.435	352.978
17	150.315	549.665	340.777	453.327	470.6	505.607	493.005	504.321	477.265	363.62	200.23	321.579
18	401.205	524.587	453.614	414.293	428.27	503.739	546.519	500.634	496.008	179.593	155.563	154.184
19	317.22	447.624	418.952	475.668	468.081	492.826	503.142	493.789	497.306	397.662	296.559	88.025
20	393.066	510.593	395.904	443.508	473.596	512.264	549.231	517.358	360.781	440.669	276.091	167.018
21	265.065	518.933	491.21	420.808	431.74	503.703	558.15	518.407	346.227	491.61	436.828	393.317
22	292.346	434.432	494.891	491.223	179.561	491.726	560.202	515.498	471.468	342.57	470.585	496.179
23	140.395	379.906	492.891	500.6	460.912	493.279	548.078	500.296	464.909	463.524	375.01	529.42
24	162.23	469.062	489.353	476.182	455.278	516.507	543.047	514.49	449.668	332.029	391.126	352.199
25	145.441	505.586	493.2	401.444	248.871	501.483	491.776	523.378	439.108	237.675	517.228	182.632
26	280.333	504.813	498.518	462.623	347.996	514.566	433.391	488.663	402.911	413.187	490.563	220.176
27	286.948	459.863	445.928	493.525	408.917	492.557	490.778	447.068	486.654	221.402	476.107	181.419
28	420.013	284.532	477.768	428.1	451.278	515.919	489.569	442.047	523.088	389.466	429.178	165.048
29	498.023	305.773	453.248	452.336	493.464		478.218	61.002	517.086	480.335	430.577	246.768
30	315.376	323.794	408.142	434.642	468.855		503.892	451.652			432.56	459.174
31				429.525			519.737				502.089	463.235
Monthly Avg.	310.8402	423.3066	432.6924	411.268	406.8334	480.0316	490.936	471.379	428.8484	353.7727	366.1765	320.9418

Avg. change of Irradiation	408.08 (W/m²)		
Monthly max.	490.93	% Monthly max.change	23.82%
Monthly min.	310.84	% Monthly min.change	20.30%
Daily max.	551.36	% Daily max.change	75.52%
Daily min.	99.885	% Daily min.change	35.11%

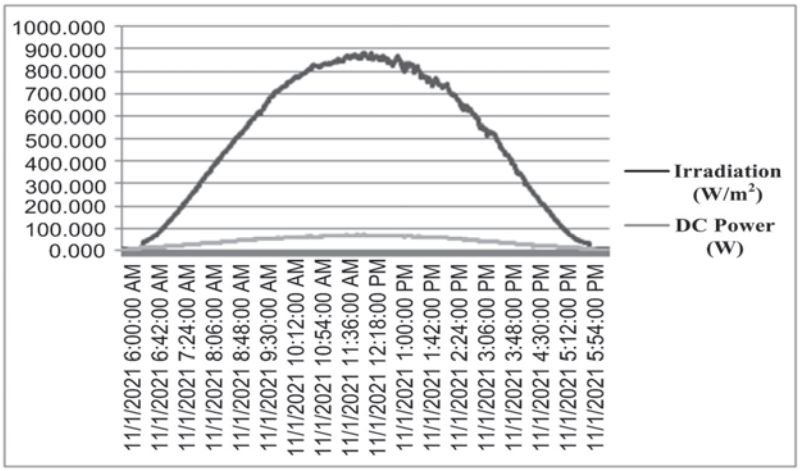

Figure 2 Normal irradiation variations on a day.

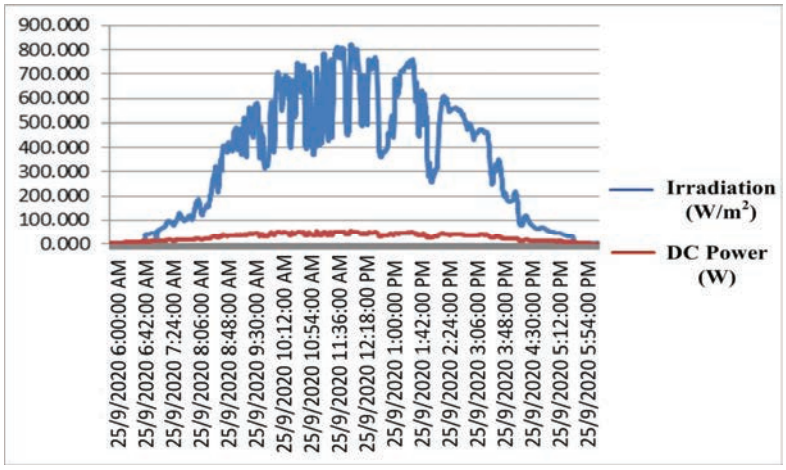

Figure 3 Severe irradiation variations on a day.

l in meters, and a is a constant parameter (s/m).

$$\tau = al \tag{1}$$

The control for ramp-rate is shown in Figure 5. At first, the inverter attempts to inject all of its power into the grid, $P_G(t) = P_{PV}(t)$. When the maximum permissible ramp rate (r_{max}) is violated, the control is activated.

$$|\Delta P_G(t)| > r_{\max} \tag{2}$$

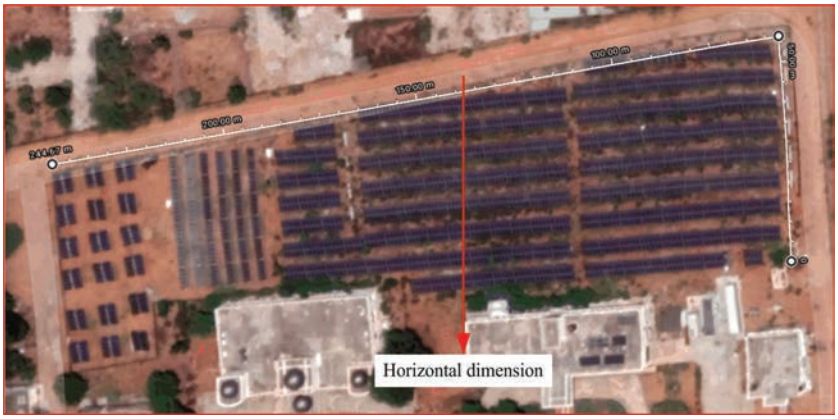

Figure 4 An aerial view of the 500 kW_P plant profile.

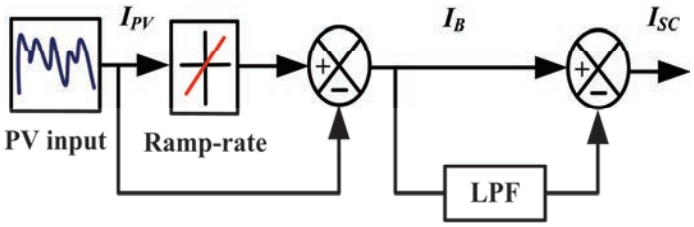

Figure 5 RRC model diagram.

The surplus or deficit power is then taken from ($P_{bat}(t) > 0$) or stored ($P_{bat}(t) < 0$) in the battery. The battery's stored energy ($E_{bat}(t)$) can be calculated by the integral of $P_{bat}(t)$ over time. As a result, the total system is easily calculated for any $P_{pv}(t)$ time series. The following Equations (3) and (4) are used to calculate the required battery power and battery energy [26]:

$$P_{bat.\max}(t) = \frac{P}{100}\left[90 - \tau r_{\max}\left(1 + \ln\frac{90}{\tau r_{\max}}\right)\right] \tag{3}$$

$$E_{bat.\max}(t) = \frac{0.9P}{3600}\left[\frac{90}{2r_{\max}} - \tau\left(1 - \exp\left\{\frac{90}{\tau r_{\max}}\right\}\right)\right] \tag{4}$$

The fluctuation of PV power generation is symmetrical due to clouds reaching and leaving the PV field. The min. to min. recorded data for fluctuating PV power is presented in Table 2.

In this design, the capacity required to equalize the PV variation is controlled and the capacity required for the most extreme fluctuations is

Table 2 500 kW_P plant min to min recorded data

Date	Time	Irradiation (W/m^2)	PV Output Power (DC) kW	Transformer Output Power (AC) kW
9/8/20	2:08:00 PM	694.17	174.9	118.86
9/8/20	2:09:00 PM	936.03	181.2	122.44
9/8/20	2:10:00 PM	958.57	182.44	126.2

calculated. Although the sign of fluctuations is unknown, the dual battery capacity is needed to be able to handle rising and falling fluctuations. However, this can be realized by monitoring the charge and discharge dynamics of the battery. The required capacity of the battery (C_{bat}) is determined using the equation below [26],

$$C_{bat} = 2E_{bat.\max}(t) \tag{5}$$

The ESS state of charge (SoC) is measured as the ratio of instant ESS energy (E_p) to rated ESS energy (E_R), which is given as:

$$SoC(t) = \frac{E_P}{E_R} \tag{6}$$

3 Configuration of Grid Connected System

The block diagram of a renewable grid-integrated system is presented in Figure 6. The system consists of PV and HESS with associated high-gain boost (HGBC) and bidirectional converters, as well as an inverter, a grid, a PLL, and a filter. Using the Phase Locked Loop (PLL), an inverter can be synchronised and its active/reactive power flow regulated by altering the feedback variables. The phase balance, voltage, and frequency of the inverter need to match the grid, hence synchronisation with the grid is necessary. There are specific techniques for this purpose. Among these, PLL is a frequently used synchronisation technique. High-frequency harmonics can be reduced with the L-C-L filter.

3.1 Control Method for the Proposed System

The control diagram for the proposed method is illustrated in Figure 7. When the output power of the PV system exceeds a defined threshold, the battery will be charged, and the battery will be discharged if the PV power generated is less than the defined value. The battery current (I_B) is calculated from the given Equation (7). The charging/discharging commands and current

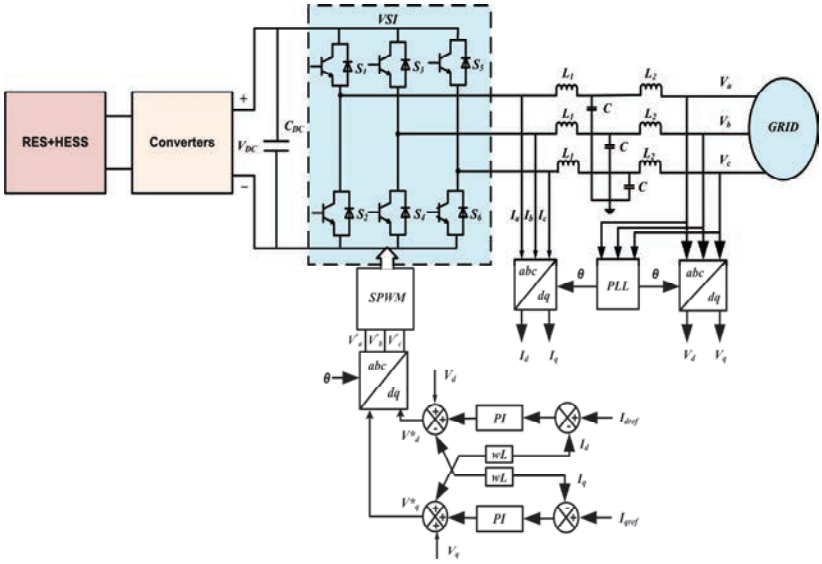

Figure 6 Block diagram of a renewable grid-integrated system.

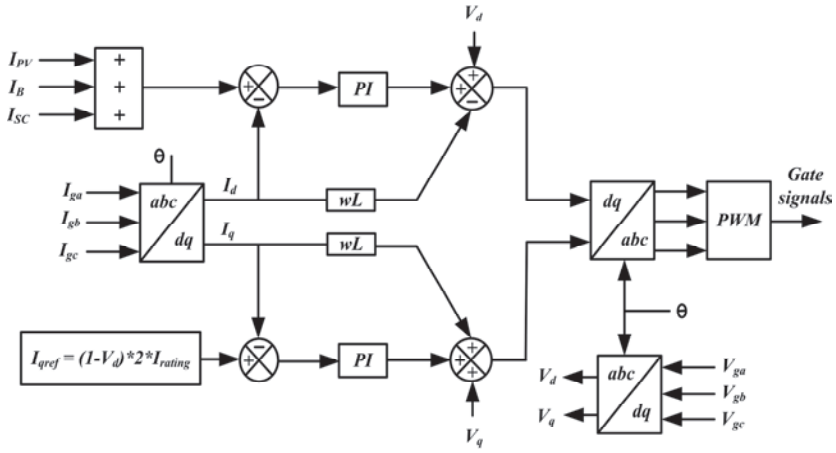

Figure 7 Control diagram of the proposed system.

reference are received by the converter controller from the system level controller. This controller implements all converter control loops, such as grid synchronisation, converter current control, and PWM pulse generation.

$$I_B = I_G - I_{PV} - I_{SC} \tag{7}$$

Several methods are available for calculating the gains of the PI controller K_p and τ. To improve the control loop performance, the PI controller must be properly tuned. The following are some of the advantages of the PI controller [27]:

1. Steady state response is good.
2. The current ripple is less pronounced.
3. The switching frequency is constant.

PI controllers can be used in either stationary or synchronous reference frames. The synchronous PI controller is a common solution for grid-connected three-phase converters because it converts the control variables to DC and reduces the steady state error in the fundamental element to zero. Depending on the criteria of the controller, the method can be chosen. Cascade control generally requires a faster reaction time in the internal loop. As a result, the internal control loop is designed to respond quickly. The main goals of the outer control loop are control and stability. The inner control loop is adjustable to a "modulus optimum" condition due to its quick response and flexibility [28], whereas the outer loop is in a "symmetrically optimum" condition to optimize system behaviour in response to disturbance signals [29].

3.1.1 Modulus optimum method

The basic transfer function (TF) is [30],

$$F = \frac{\omega_0^2(ks + \omega_0)}{s^2(s + k\omega_0)} \tag{8}$$

Where *k* is a constant that can be symmetric around $\omega = \omega_0$. The open-loop TF of the system is given below in equation [31],

$$G_{OL} = \left(K_P \frac{1 + s\tau}{s\tau}\right)\left(\frac{1}{1 + sT_s}\right)\left(\frac{V_m}{s}\right) \tag{9}$$

The Equations (8) and (9) are modified as follows:

$$\frac{KV_m}{T_s}\frac{\left(s + \frac{1}{\tau}\right)}{s + \frac{1}{T_s}} = \frac{KV_m}{aT_s}\frac{\left(as + \frac{a}{\tau}\right)}{s^2\left(s + \frac{1}{T_s}\right)} \tag{10}$$

Whereas a and T_s are the normalization factor and sampling period, the Equation (11) provides the ensuing identifications. Rewriting the above

equation, the following controller gains are obtained:

$$\omega_c = a\frac{1}{T_s} \tag{11}$$

$$\tau = a^2 T_s \tag{12}$$

$$K = \frac{1}{aV_m T_s} \tag{13}$$

The second order system is measured between bandwidth (ω_b) and crossover frequency (ω_c) and is almost constant for the closed loop system [32].

$$0.6 < \frac{\omega_c}{\omega_b} < 0.8 \tag{14}$$

3.1.2 Transfer function of the current controller

The PI current controller loop diagram is presented in Figure 8.

The current controller open loop transfer function is given as follows [33]:

$$G_{OL}(s) = \frac{1}{2T_a}\left(\frac{1}{s(1+\tau_a s)}\right) \tag{15}$$

The PI controller parameters are determined by the modulus optimum tuning criteria for this system [33].

$$K_p = \frac{\tau_{pu} R_{pu}}{2T_a} \tag{16}$$

$$T_i = \tau_{pu} \tag{17}$$

Where T_i and K_p are the integral time constant and proportional gain of the PI regulator, τ is a time constant, and T_a is the time delay of the converter.

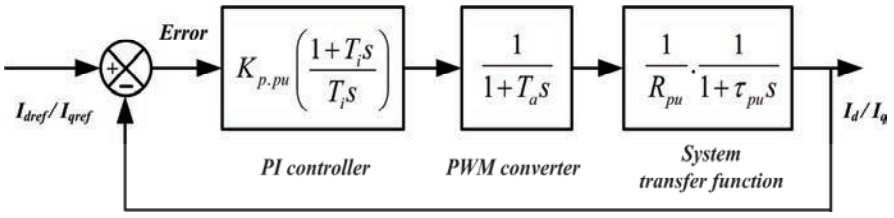

Figure 8 PI current control block diagram in Pu.

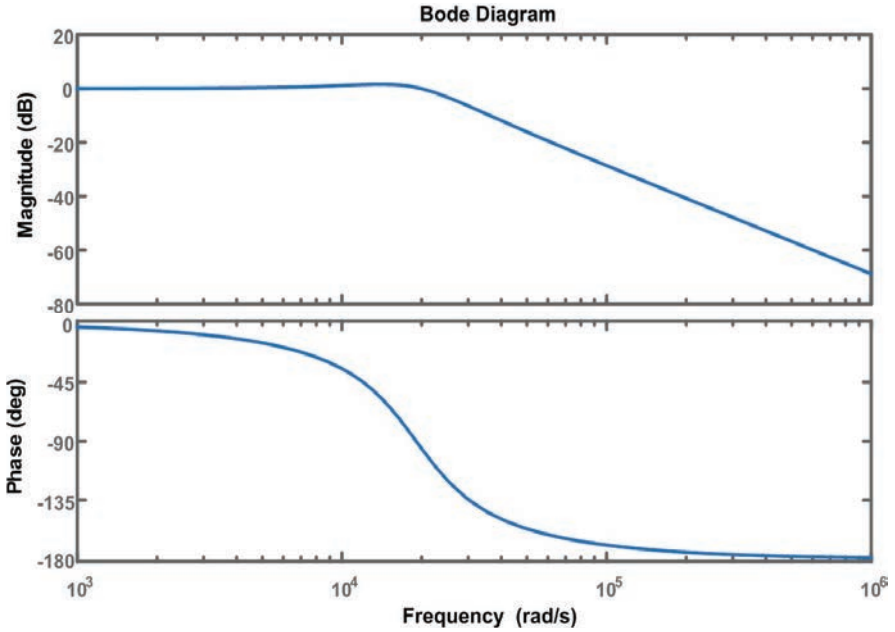

Figure 9 Bode plot of the proposed current control system.

Hence, the open loop ($G_{OL}(s)$) and closed loop ($G_{CL}(s)$) current control loop transfer functions are given by this tuning criterion as follows:

$$G_{OL}(s) = \frac{1}{2T_a}\left(\frac{1}{s(1+\tau_a s)}\right) \tag{18}$$

$$G_{CL}(s) = \frac{1}{2T_a^2 s^2 + 2T_a s + 1} \tag{19}$$

The bode plot of the proposed current control system is presented in Figure 9. For different values of K_p while designing PI for the step response, the following constraints must be considered [34],

- To obtain a less oscillatory response, phase margin should be high.
- τ should be low, to get less settling time.
- Bandwidth and phase margin are affected by the value of K_p.

To get maximum phase margin, the ω_c should be around grid frequency (50 Hz). The closed-loop system (CLS) also has the features of a low pass filter (LPF) with a band width of $\omega_b \approx \omega_c/0.7 \approx 71$ HZ.

4 Results and Discussion

The HIL system parameters are presented in Table 3. The HIL test bench in the laboratory is equipped with OPAL-RT stacks, as shown in Figure 10. Stacks can quickly create prototypes and hardware synchronization. The plant and controller are installed on the OPAL-RT system in the RT-LAB environment to operate at physical clock time. To validate the system

Table 3 System parameters

Specifications	Values
PV Capacity (P_{PV})	500 kW_p
Time constant (τ)	2 sec
Shortest dimension of PV plant (l)	56.6 m
Grid Voltage (V_L)	415 V (rms)
DC Link Voltage (V_{DC})	700 V
Inverter Power (P)	523 kW
Ramp rate value (r_{max})	0.166
Battery power ($P_{bat.max}$)	462 kW
Battery energy ($E_{bat.max}$)	35.5 kWh
Battery capacity (C_{bat})	71 kWh
Rated voltage (V_C)	16
No. of SCs in series	2
Rated capacitance (C_{rated})	58 F
Frequency (f)	50 Hz
Filter values	$L_1 = 51\ \mu$H, $L_2 = 0.7\ \mu$H, $C = 452\ \mu$F

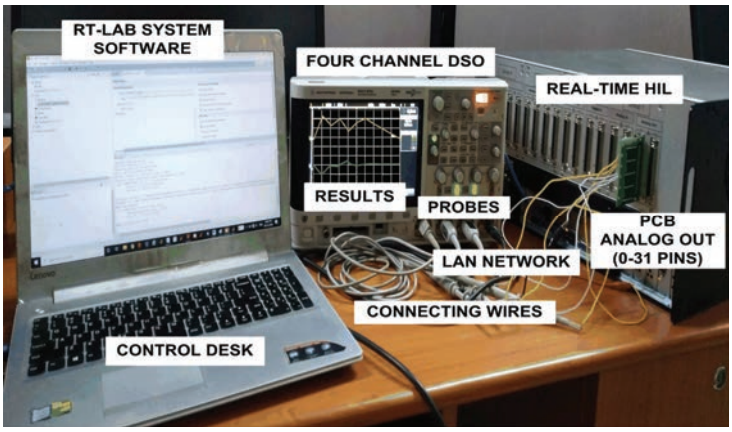

Figure 10 HIL Results set-up.

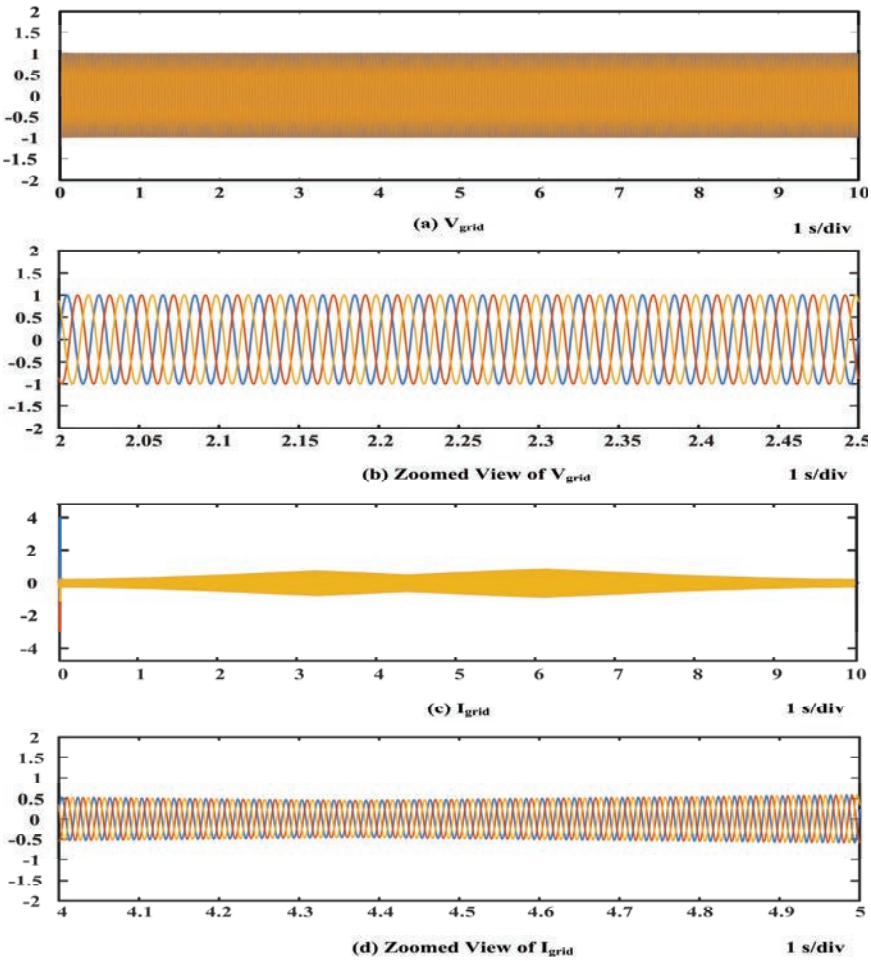

Figure 11 Simulation results for grid voltage (V_{grid}) and grid current (I_{grid}) in Pu.

results, the OP5700 HIL test bench, RT-LAB system software, MSOX3014A, PCBE06-0560 control board, probes, and connecting wires are used.

Case i: When I_d = Active; $I_q = 0$

Case ii: When I_d = Active; I_q = *(1-V_d)*2*I_{rating}*

Figures 11(a) and (c) show the simulated results of grid voltage and current values in per-unit (Pu) terms. The zoomed values of grid voltage and current are presented in Figures 11(b) and (d). The waveforms can be seen to

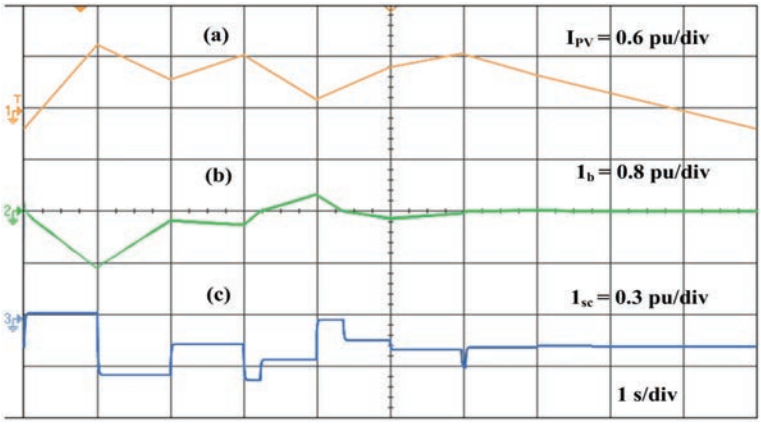

Figure 12 HIL results: (a) PV, (b) battery response to the grid, and (c) SC currents in Pu.

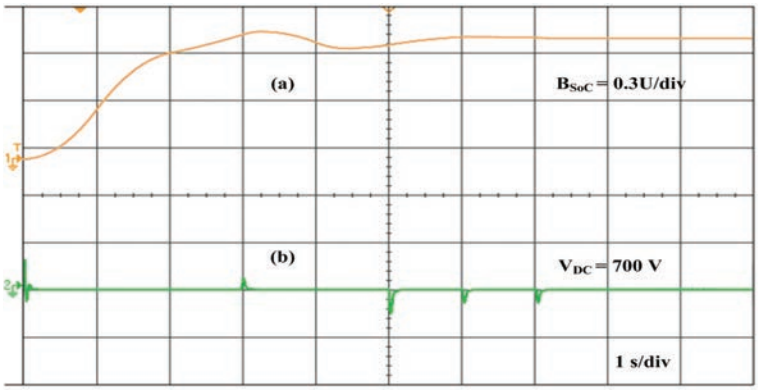

Figure 13 HIL results: (a) battery SOC, and (b) DC-bus voltage.

be sinusoidal in nature. The variation in the PV's current profile is depicted in Figure 12(a). The output of the BESS current with respect to the grid is presented in Figure 12(b). As shown in Figure 12(b), the power injected into the grid by PV with ESS changes gradually when the irradiance fluctuates. The response of the SC current is presented in Figure 12(c). The sudden variations in battery current can cause stress on the battery and reduce its lifetime. The SC responds to these variations by removing transients from the battery. As a result, the life of the battery device has increased. Figure 13(a) shows the battery state of charge (SoC), and the initial SoC is considered to be 70%. The battery SoC responds to the charging and discharging cycles of the battery. Figure 13(b) depicts the constant DC link voltage. The zoomed view

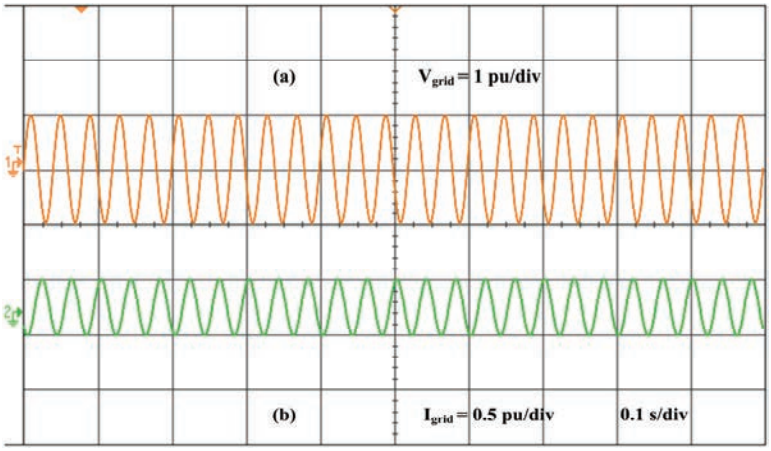

Figure 14 HIL results: Zoomed view of (a) grid voltage (V_{grid}), and (b) grid current (I_{grid}).

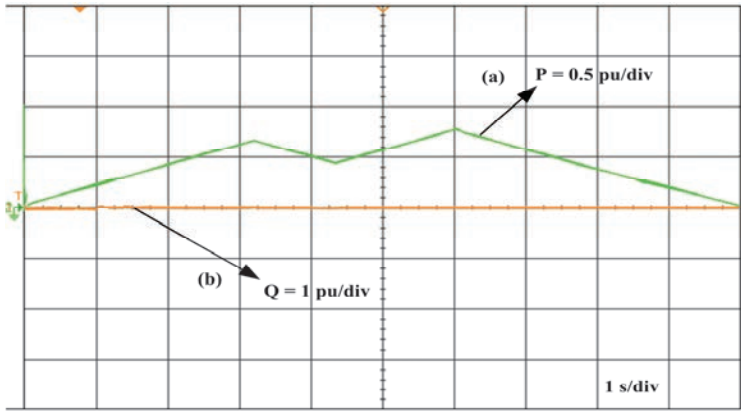

Figure 15 HIL results: (a) active, and (b) reactive powers in Pu.

of grid voltage and current of HIL results is presented in Figure 14(a) and (b). The active and reactive powers are shown in Figure 15(a) and (b). In this case, the active power response is based on the controller's battery response to the grid. Because there is no variation in the amplitude of the voltage, the reactive power is not shown. As a result, the control is deactivated, and $I_q = 0$.

Power outages and voltage fluctuations can cause distributed generation systems (DG) to be quickly disconnected from the grid, increasing their use in power distribution networks. Hence, DG units are required to assist the grid in fault situations. The significance of these requirements is fault ride-through

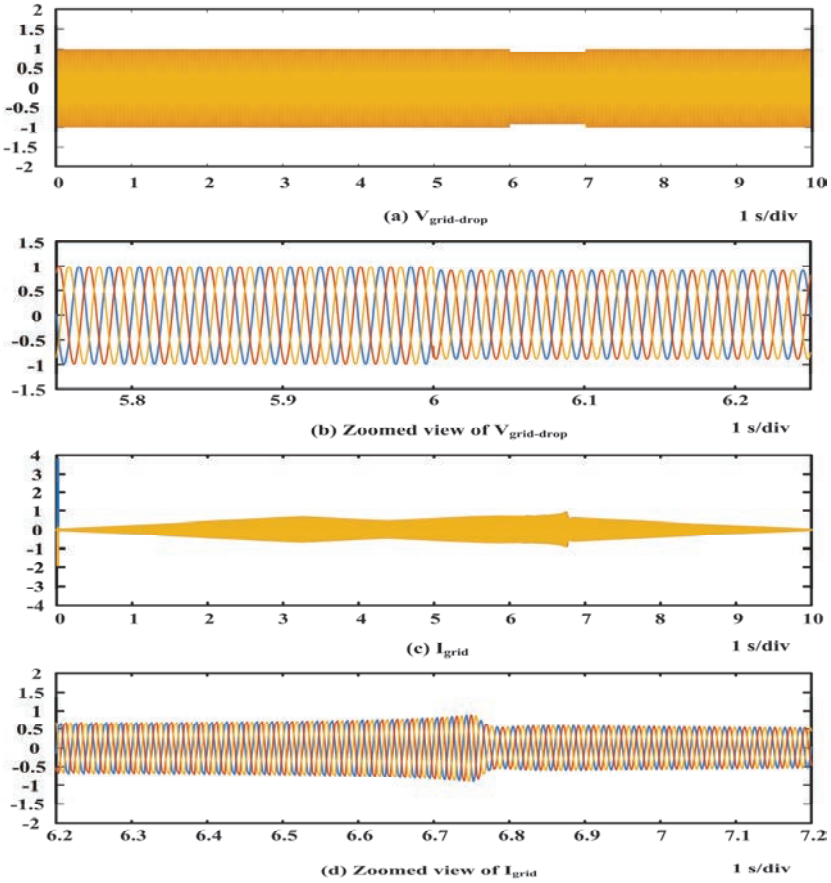

Figure 16 Simulation results for grid-voltage ($V_{grid-drop}$) and grid current (I_{grid}) in Pu.

capability (FRT). It basically allows the controller design in such a way that RES can remain associated with the system during abnormal operation conditions and contribute to voltage support during and after abnormal operating conditions [35–37]. In this case, a reference current generation method is used in the proposed FRT control strategy to eliminate oscillations in the active power during unbalanced voltage dips and sustain the stable DC-link voltage. As shown in Figure 16(a), the amplitude of the voltage decreases during an interval of 6–7 s to its original value. The response of the grid current is presented in Figure 16(c). The zoomed values of grid voltage and current are shown in Figures 16(b) and (d). The HIL results of the grid voltage and current are illustrated in Figure 17(a) and (b). In a fault condition,

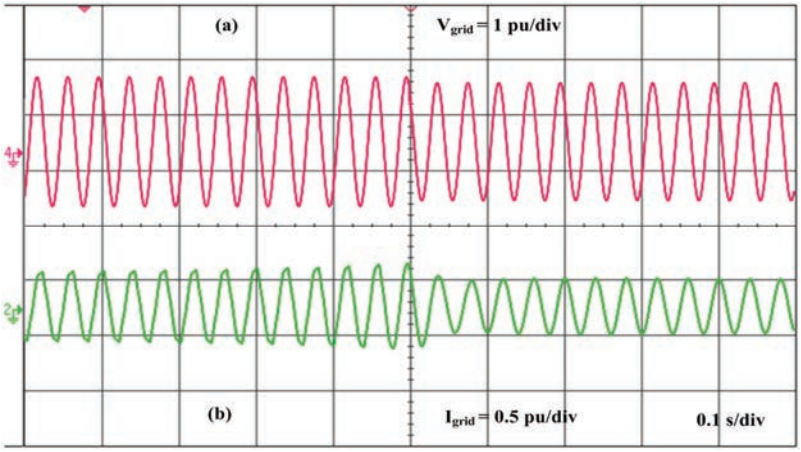

Figure 17 HIL results: Zoomed view of (a) grid voltage ($V_{grid-drop}$), and (b) grid current (I_{grid}).

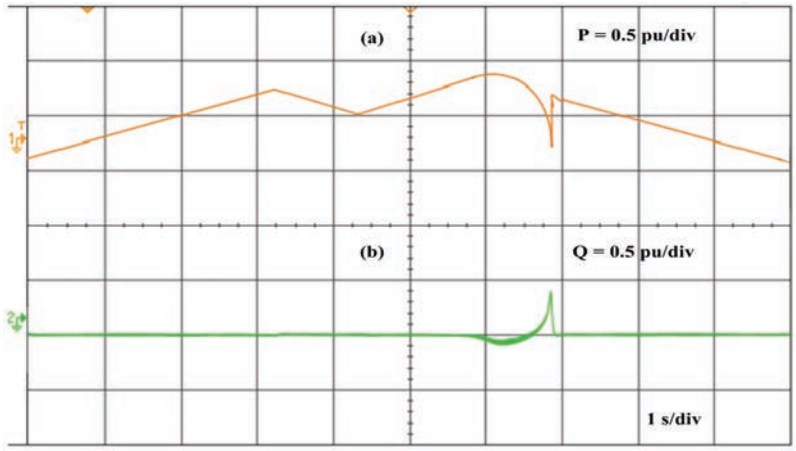

Figure 18 HIL results: (a) active, and (b) reactive powers.

active power is reduced to its original value in a time period of 6 to 7 s in Figure 18(a). The reactive power must be regulated effectively to maintain a constant grid voltage during transient faults. As a result, the control is activated, and the reactive component of power is compensated for during the 6–7 s interval depicted in Figure 18(b). This assists the grid in maintaining voltage stability in the event of a fault. Reactive power is supplied to assist with voltage recovery based on the depth of grid voltage sags.

5 Conclusion

The proposed system is used to dynamically charge the integrated BS to mitigate voltage rises during midday and discharge it during the night peak hours and to simultaneously charge or discharge the integrated SC storage in order to regulate the rapid fluctuations in the PV converter of a specific magnitude. An energy sharing method between BS and SC storage is presented to provide continuous control of fast variations during cloud passage. Hence, solar PV with a capacity of 500 kW_p requires only 71 kWh of battery energy to smooth out the output of PV variations due to irradiation and temperature. The proposed control allows the system to generate reactive power to assist the grid during a fault and also assists the grid in maintaining voltage stability during a fault. Reactive power is provided to assist with voltage recovery based on the depth of grid voltage sags. After the grid voltage is restored to its nominal value, the RES system delivers real power as quickly as possible to keep a real power balance, thus helping to restore the entire system. The proposed FRT capability system is based on the reference current generation method and it eliminates active power oscillations during unbalanced voltage dips. The performance of the solar energy generated by controlling its ramp rate smoothly improves grid stability and reduces the need for energy storage. The system's performance was evaluated using the HIL test bench. As a result, the power injected into the grid through PV with HESS changes gradually during a sudden variation in irradiation levels.

Acknowledgements

This work was supported by the Department of Science and Technology (DST), Government of India (GOI) with the project grant SR/FST/ETI-420/2016(C) under FIST scheme.

References

[1] G. Kumar, R. Sarojini, K. Palanisamy, S. Padmanaban, J. Holm-Nielsen, "Large Scale Renewable Energy Integration: Issues and Solutions," *Energies* vol. 12, no. 10, pp. 1–17, 2019.

[2] P. Ariyaratna, K. M. Muttaqi, D. Sutanto, "A novel control strategy to mitigate slow and fast fluctuations of the voltage profile at common coupling Point of rooftop solar PV unit with an integrated hybrid energy storage system," *Journal of Energy Storage*, vol. 20, pp. 409–417, 2018.

[3] J. Marcos, O. Storke, L. Marroyo, M. Garcia, and E. Lorenzo, "Storage requirements for PV power ramp-rate control," *Sol. Energy*, vol. 99, pp. 28–35, 2014.

[4] G. V. Brahmendra Kumar and K. Palanisamy, "A Review on Microgrids with Distributed Energy Resources," 2019 Innovations in Power and Advanced Computing Technologies (i-PACT), 2019, pp. 1–6.

[5] B. M. Sanandaji, T. L. Vincent and K. Poolla, "Ramping Rate Flexibility of Residential HVAC Loads," in *IEEE Transactions on Sustainable Energy*, vol. 7, no. 2, pp. 865-874, 2016, doi: 10.1109/TSTE.2015.2497236.

[6] L. Marroyo, I. De Parra, J. Marcos, and M. Garcı, "Control strategies to use the minimum energy storage requirement for PV power ramp-rate control," *Sol. Energy,* vol. 111, pp. 332–343, 2015.

[7] V. B. K. Gundumalla and S. Eswararao, "Ramp Rate Control Strategy for an Islanded DC Microgrid with Hybrid Energy Storage System," 2018 4th International Conference on Electrical Energy Systems (ICEES), 2018, pp. 82–87.

[8] G. V. B. Kumar and K. Palanisamy, "Interleaved boost converter for renewable energy application with energy storage system," In Proceedings of the 2019 IEEE 1st International Conference on Energy, Systems and Information Processing (ICESIP), 2019, pp. 1–5.

[9] R. Van Haaren, M. Morjaria, and V. Fthenakis, "Empirical assessment of short-term variability from utility-scale solar PV plants," *Progress in Photovoltaics*, vol. 22, pp. 548–559, 2012.

[10] G. V. Brahmendra Kumar and K. Palanisamy, Review of energy storage system for microgrid, *Microgrid Technologies*, *Wiley,* vol. 31, no. 9, pp. 57–90, 2021.

[11] G. V. B. Kumar and K. Palanisamy, "A Review of Energy Storage Participation for Ancillary Services in a Microgrid Environment," *Inventions,* vol. 5, no. 4, pp. 1–36, 2020.

[12] M. J. E. Alam, K. M. Muttaqi, D. Sutanto, "A Novel Approach for Ramp-Rate Control of Solar PV Using Energy Storage to Mitigate Output Fluctuations Caused by Cloud Passing," *IEEE Trans. Energy Convers*., vol. 29, no. 2, pp. 507–518, 2014.

[13] S. A. Abdelrazek and S. Kamalasadan, "Integrated PV Capacity Firming and Energy Time Shift Battery Energy Storage Management Using Energy-Oriented Optimization," in *IEEE Transactions on Industry Applications*, vol. 52, no. 3, pp. 2607–2617, 2016, doi: 10.1109/TIA.2016.2531639.

[14] H. Beltran, E. Bilbao, E. Belenguer, I. Etxeberria-Otadui and P. Rodriguez, "Evaluation of Storage Energy Requirements for Constant Production in PV Power Plants," in IEEE Transactions on Industrial Electronics, vol. 60, no. 3, pp. 1225–1234, March 2013, doi: 10.1109/TIE.2012.2202353.

[15] J. Schnabel, S. Valkealahti, "Energy storage requirements for PV power ramp rate control in northern Europe," *Int. J. Photoenergy*, pp. 1–11, 2016. https://doi.org/10.1155/2016/2863479.

[16] M. M. Id and Á. Miguel, "A Grid Connected Photovoltaic Inverter with Battery-Supercapacitor Hybrid Energy Storage," *Sensors*, vol. 17, no. 8, 2017, doi: 10.3390/s17081856.

[17] W. Jiang, L. Zhang, H. Zhao, H. Huang and R. Hu, "Research on power sharing strategy of hybrid energy storagesystem in photovoltaic power station based on multi-objective optimisation," in *IET Renewable Power Generation*, vol. 10, no. 5, pp. 575–583, 2016, doi: 10.1049/iet-rpg.2015.0199.

[18] R. Perez, S. Kivalov, J. Schlemmer, K. Hemker, and T. E. Hoff, "Short-term irradiance variability: Preliminary estimation of station pair correlation as a function of distance," *Sol. Energy*, vol. 86, no. 8, pp. 2170–2176, 2012.

[19] H. Beltran, I. Tomás García, J. C. Alfonso-Gil and E. Pérez, "Levelized Cost of Storage for Li-Ion Batteries Used in PV Power Plants for Ramp-Rate Control," in *IEEE Transactions on Energy Conversion*, vol. 34, no. 1, pp. 554–561, 2019, doi: 10.1109/TEC.2019.2891851.

[20] G. V. B. Kumar, K. Palanisamy and E. D. Tuglie, "Energy Management of PV-Grid-Integrated Microgrid with Hybrid Energy Storage System," 2021 IEEE International Conference on Environment and Electrical Engineering and 2021 IEEE Industrial and Commercial Power Systems Europe (EEEIC / I&CPS Europe), 2021, pp. 1–6.

[21] R. Perez, T. Hoff, J. Dise, D. Chalmers, and S. Kivalov, "The cost of mitigating short-term PV output variability," *Energy procedia*, vol. 57, pp. 755–762, 2014.

[22] G. Anilkumar, A. Chakradhar, G. V. Brahmendra Kumar, and K. Palanisamy, "Resource assessment and energy yield estimation for 160 MW solar-wind hybrid project using system advisory model," *IOP Conf. Ser. Mater. Sci. Eng.*, vol. 937, p. 012020, 2020.

[23] M. García, L. Marroyo, E. Lorenzo, J. Marcos, and M. Pérez, "Solar irradiation and PV module temperature dispersion at a large-scale PV plant," *Progress in Photovoltaics*, vol. 33, no. 10, pp. 1381–1389, 2014.

[24] G. V. B. Kumar, P. Kaliannan, S. Padmanaban, J. Holm-Nielsen, F. Blaabjerg, "Effective Management System for Solar PV Using Real-Time Data with Hybrid Energy Storage System," *Applied Sciences*, vol. 10, no. 3, pp. 1–15, 2020.

[25] V. T. Tran, M. R. Islam, D. Sutanto and K. M. Muttaqi, "Mitigation of Solar PV Intermittency Using Ramp-Rate Control of Energy Buffer Unit," in *IEEE Transactions on Energy Conversion*, vol. 34, no. 1, pp. 435–445, 2019, doi: 10.1109/TEC.2018.2875701.

[26] G. V. Brahmendra Kumar, G. A. Kumar, S. Eswararao and D. Gehlot, "Modelling and Control of BESS for Solar Integration for PV Ramp Rate Control," 2018 International Conference on Computation of Power, Energy, Information and Communication (ICCPEIC), 2018, pp. 368–374.

[27] N. Beg, A. Rahmoun, A. Armstorfer, A. Rosin and H. Biechl, "Determination methods for controller parameters of back-to-back converters in electric power grids," 2016 Electric Power Quality and Supply Reliability (PQ), pp. 157–164, 2016. doi: 10.1109/PQ.2016.7724106.

[28] S. Chamraz and R. Balogh, "Potential of the Optimum Modulus Method," 2016 Cybernetics & Informatics (K&I), pp. 1–6, 2016. doi: 10.1109/CYBERI.2016.7438622.

[29] V. K. Pavuluri, X. Wang, J. Long, G. Zhuo and W. Lian, "Field Oriented Control of Induction Motors Using Symmetrical Optimum Method with Applications in Hybrid Electric Vehicles," 2015 IEEE Vehicle Power and Propulsion Conference (VPPC), pp. 1–6, 2015. doi: 10.1109/VPPC .2015.7352948.

[30] N. Radimov, S. Liu and X. Wang, "Extended Modulus Optimum Method for Off-Grid Inverter's Voltage Control System," 2019 IEEE Canadian Conference of Electrical and Computer Engineering (CCECE), pp. 1–5, 2019. doi: 10.1109/CCECE.2019.8861801.

[31] J. Lin and S. Li, "Optimal parameters selection to satisfy optimum modulus theory," 2010 Chinese Control and Decision Conference, pp. 1135–1140, 2010. doi: 10.1109/CCDC.2010.5498145.

[32] D. Tomas and O. Stepan, "Advanced PID tuning based on the modulus optimum method for real systems," *AIP Conference Proceedings*, vol. 1836, no. 020060, pp. 1–6, 2017. https://doi.org/10.1063/1.4982000.

[33] A. D. Giles, L. Reguera and A. J. Roscoe, "Optimal controller gains for inner current controllers in VSC inverters," International Conference on

Renewable Power Generation (RPG 2015), 2015, pp. 1–6, doi: 10.1049/cp.2015.0391.

[34] J. Cvejn, "PI/PID controller design for FOPDT plants based on the modulus optimum criterion," 2011 12th International Carpathian Control Conference (ICCC), Velke Karlovice, pp. 60–65, 2011. doi: 10.1109/CarpathianCC.2011.5945816.

[35] V. Gevorgian and S. Booth, "Review of PREPA Technical Requirements for Interconnecting Wind and Solar Generation," pp. 1–72, 2013. https://www.nrel.gov/docs/fy14osti/57089.pdf.

[36] K. Prompinit and S. Khomfoi, "Ramp rate consideration of a BESS using active power control for PV generation," 2015 18th International Conference on Electrical Machines and Systems (ICEMS), pp. 1676–1680, 2015. doi: 10.1109/ICEMS.2015.7385310.

[37] M. Chamana, B. H. Chowdhury and F. Jahanbakhsh, "Distributed Control of Voltage Regulating Devices in the Presence of High PV Penetration to Mitigate Ramp-Rate Issues," in *IEEE Transactions on Smart Grid*, vol. 9, no. 2, pp. 1086–1095, 2018. doi: 10.1109/TSG.2016.2576405.

Biographies

G. V. Brahmendra Kumar received the bachelor's degree in electrical and electronics engineering and the master's degree in renewable energy from JNT University, Kakinada, India, in 2015 and 2018. He is currently working toward a Ph.D. degree with the Smart-Grid Research Lab at the School of Electrical Engineering, Vellore Institute of Technology, Vellore, India. His research interests include microgrid power management strategies, power quality, hybrid energy storage systems, grid integration of renewable energy sources, and power converter applications in microgrids.

K. Palanisamy received the bachelor's degree in electrical engineering from the KSR College of Technology, India, in 2000, the master's (Hons.) degree in Applied Electronics from the Coimbatore Institute of Technology, India, in 2004, and the Ph.D. degree in electrical engineering from Vellore Institute of Technology, Vellore, India, in 2013. He is currently a Deputy Director-Electrical Maintenance and Projects, Associate Professor of Energy and Power Electronics Division and head of "centre for smart grid technology" at Vellore Institute of Technology between 2007 to till date. From 2016 to 2018 he was a head of the department Energy and Power Electronics Division. He has authored over 108 scientific papers in referred conference proceedings and international journals in the field of renewable energy, battery energy storage, multilevel converters and power quality. He is a certified Energy Auditor by the Bureau of Energy Efficiency, Government of India. He has taken up various consultancy projects in energy efficiency and power quality improvement.